Article

Programmable Complex Shape Changing of Polysiloxane Main-Chain Liquid-Crystalline Elastomers

Yuhe Zhang [1,+], Xiuxiu Wang [1,+], Wenlong Yang [2], Huixuan Yan [1], Xinyu Zhang [1], Dongxu Han [1], Yifan He [3], Chensha Li [1,*] and Liguo Sun [4,*]

[1] Key Laboratory of Functional Inorganic Material Chemistry, Ministry of Education of the People's Republic of China, Heilongjiang University, Harbin 150080 P. R China;
[2] Department of Applied Science, Harbin University of Science and Technology, Harbin,150080, P. R China;
[3] Institute of regulatory science, Beijing Technology and Business University, Beijing 100048 P. R. China;
[4] Key Laboratory of Chemical Engineering Process and Technology for High-Efficiency Conversion School of Chemistry and Material Science, Heilongjiang University, Harbin 150080, P. R. China;
* Correspondence: to: Chensha Li, lichensha@hlju.edu.cn; Liguo Sun, 2004087@hlju.edu.cn;
+ These authors contributed equally to this work)

Abstract: Liquid crystal elastomers (LCEs) are shape morphing materials whose large and reversible shape transformation results from the coupling between the mobile anisotropic properties of liquid crystal (LC) units and the rubber elastic of polymer networks. Their shape changing behaviors under the stimuli are largely directed by LC orientations, and therefore various strategies have been developed to spatially modulate the LC alignments. But most of the methods suffer from complex fabrication technologies or intrinsic limitations in applicability. To address this issue, programmable complex shape changes in some types of LCEs, such as polysiloxane side-chain LCEs or thiol-acrylate main-chain LCEs, etc, have been achieved by using a mechanical alignment programming process coupled with two-step crosslinking. Here, we report a polysiloxane main-chain LCE with programmable 2D and 3D shape changing performances achieved by mechanically programming the polydomain LCE between the two crosslinking steps. The resulting LCEs exhibited reversible thermal induced shape transformation between the initial and programmed shapes due to the two-way memory between the first network structure and the second network structure. Our work would be potential for expanding the applications of LCE materials in actuators, soft robotics and smart structures where arbitrary and easily programmed shape morphings are needed.

Keywords: Polysiloxane liquid crystalline elastomer; Programmable shape morphing; Two-way network memory; Mechanical programming process; Two-step crosslinking

1. Introduction

Liquid crystalline elastomers (LCEs), a class of outstanding stimuli-responsive materials, are liquid crystal (LC) moieties incorporated polymers with lightly crosslinked networks, in which the LC moieties with predesigned orientations are covalently bonded on side of polymer backbones (side-chain LCEs) or directly linked into to the polymer backbones (main-chain LCEs) [1-6]. The synergy of self-organization property of LC systems and polymeric network elasticity endows the LCEs with the function of behaving reversible, large and anisotropic dimensional change upon the application of external energy stimuli [1-6], and thus makes them to be appealing candidate in diverse application fields including soft actuators [7-16], soft robotics [17-24], artificial muscles [25-32], and biomedical devices [33-42], *etc*.

The shape changes of LCEs are governed by a coupling between the LC orientations and anisotropic polymer networks, and rely on a reversible nematic-isotropic transition associated with LC moieties. By being heated above the nematic-isotropic transition temperature (T_{ni}), the alignment order of LC moieties is disrupted, and the LCE transfers from nematic LC phase into isotropic state and drives the macroscopic shape change. Upon the

 doi:10.20944/preprints202304.1181.v1

cooling below T_{ni}, the alignment order and LC phase are recovered, and the LCE reverts to its initial shape [1]. The spatial distribution of LC molecule alignment is responsible for the shape-shifting behavior of LCEs. Uniaxial alignment can only lead to simple shape morphing modes such as in-plane contraction/elongation or bending/unbending [1-3] which cannot meet the development requirement towards versatile 3D shape morphing modes.

More diverse shape morphings in LCE materials can be achieved by imprinting complex LC orientations into LCE networks. A variety of in situ LC molecule alignment techniques, such as surface treatment [43-47], microfluidic process [48-50], photoalignment [6, 51-53], and the use of magnetic field [54-56] or electric field [1], have been employed to achieve the spatial control of LC alignment which can bring about complex shape morphings. Recently, direct ink writing 3D printing has been introduced to fabricate LCEs with programmed spatial LC orientations induced by shear stress during filament-extrusion, and the resulting 3D shape changing performances [8, 57-61]. These strategies have their respective benefits, but often face the problems of complication and application limitation, such as tedious orientation technology, monotonous geometries and sophisticated setups, *etc*, for reason that they generally require determining the LC orientation profiles for producing the desired shape changes. In recent years, dynamic covalent bonds have been introduced into LCEs to prepare covalent adaptable LCE networks which enable the programmability of LC orientations. When a LCE is subjected to mechanical load, an applied stimulus, such as heating or UV irradiation, can trigger an exchange reaction in which the covalent bonds undergo cleavage and rearrangement. After removal of the stimulus, the LCE retains the mechanically programmed alignments of LC moieties in the network [17, 62-68]. The approach of incorporating dynamic covalent bonds into LCEs has shown to be robust and facile for the fabrication of LCE materials with complex shapes and programmable shape morphing behaviors. However, external stimuli and catalysts or initiators are often needed to drive the bond exchange reaction, and thus the materials' performances may be prone to deteriorate after they have been used repeatedly.

Historically, Finkelmann *et al*, first developed mechanical alignment to prepare uniaxially aligned monodomain LCEs [69]. Their way was based on two-step crosslinking combining with a mechanical alignment, and has been commonly adopted in the preparation of many uniaxially aligned LCE materials. In our previous work, we first achieved direct programmable complex 2D shape changing performance in a classical side-chain polyhydrosiloxane LCE by using this way [70]. The reason for such performance should be due to the two-way memory between the first network structure and the second network structure formed in the two-step crosslinking process. The two-way network memory induced two-way shape memory. During the thermal-triggered phase transition between LC phase and isotropic state, the LCE could reversibly change between the initial shape formed in the first crosslinking step and any another shape programmed by mechanical process and fixed by the second crosslinking step [70]. This demonstrated performance was like shape memory polymers (SMPs), whose stimuli-responsive shape changes can be readily achieved by utilizing the "mechanical programming processes" [71]. A temporary shape can be directly imprinted in a SMP under an external stress and elevated temperature, and remained after quenching. Upon heating, the SMP recovers to its initial shape and the programmed shape transformation is completed. From then on, researchers have achieved "SMP-liked" programmable complex shape changes in some other types of LCEs, such as thiol-acrylate main-chain LCEs and alkylamine-acrylate main-chain LCEs, *etc*, by using the methods based on two-step crosslinking combining with a mechanical alignment [21, 72-74]. In their methods, photo-crosslinking was employed as the second step crosslinking to lock the LC orientations in LCE matrices and the mechanically programmed shapes in order to impart reversible and programmable shape morphing behavior. However, light-initiated polymerization reactions may be not very convenient in constructing complex 3D structures due to the shallow penetration depth and self-shadowing effect of the lights.

 doi:10.20944/preprints202304.1181.v1

In this work, we report an achievement of direct programming complex reversible shape morphings in polysiloxane main-chain LCEs by using an approach based on two-step crosslinking combining with a mechanical alignment. Main-chain LCEs can exhibit much higher mechanical and strain actuation properties compared to side-chain LCEs due to direct coupling of the LC moieties to polymer backbone chains [1], and thus provided more sophisticated 3D programmable shape morphing behaviors compared to our first side-chain LCEs [70]. In the first step crosslinking, a partially crosslinked polydomain LCE was generated through the hydrosilylation polyaddition and crosslinking reaction driven by ultrasonics sonochemistry process [75]. Then *via* stretching, pressing, stamping or embossing, it was mechanically programmed to be another 1D, 2D or 3D-shaped LCE. Lastly, the LC alignment distribution and the programmed shape of the material was locked by the second step thermal crosslinking. Reversible transformation of the LCEs between the initial shapes and the programmed shapes were successfully demonstrated when exposed to heat, resulted in direct mechanically programmed shape morphings. This facile and versatile strategy of realizing programmable shape morphing performance utilized the property of two-way network memory, necessitates no foresight of the required profile of LC orientation and is not limited to the fabricated shapes of LCE materials, and thus can be potential to facilitate the design and application of LCE materials in sophisticated smart devices and multi-functional structures where arbitrary and easily programmed shape morphings are needed.

2. Experiment section

2.1. Material preparations

The mesogens (LC units), which were "4-(but-3-en-1-yloxy)phenyl 4-(but-3-en-1-yloxy)benzoate (LC44)" and "4-(hex-5-en-1-yloxy)phenyl 4-(hex-5-en-1-yloxy)benzoate (LC66)", were synthesized as our previous reported work [76]. The chain extender, cyclic siloxane crosslinker and commercial platinum catalyst, which were respectively "1, 1, 3, 3-teramethydisiloxane (TMDSO)", "2, 4, 6, 8, 10-pentamethyl-1, 3, 5, 7, 9, 2, 4, 6, 8, 10-pentaoxapentasilecane (PMPOPS)", and "dichloro (1,5-cyclooctadiene) platinum (II) ($Pt(COD)Cl_2$)", were purchased from Aldrich (St Louis, USA). The catalyst solution was prepared as our previous reported work [75].

The precursor reactant solutions were prepared by dissolving mesogenic monomer "LC44" and "LC66", chain extender "TMDSO" and crosslinker "PMPOPS" in toluene solvent. Table 1 lists the used reactant amounts, the volumes of toluene solvent and catalyst solution for the preparation of polysiloxane main-chain LCEs with 1D, 2D or 3D programmed shapes. The preparation processes of the LCEs are described in "S-Ⅰ", "S-Ⅱ" and "S-Ⅲ" of the ESI†, and illustrated in Scheme S1 to Scheme S6 of the ESI†.

Table 1. The used amounts of precursor reactants for LCE preparations.

Programmed shape	Reactant amounts					
	LC44	LC66	TMDSO	PMPOPS	Toluene solvent (μL)	Catalyst solution (μL)
1D shape: Strip shape	0.1692g (0.5mmol)	0.1973g (0.5mmol)	0.1072g (0.8mmol)	0.0268g (0.08mmol)	1300	25
1D shape: Rod shape	0.0423g (0.125mmol)	0.04933g (0.125mmol)	0.0268g (0.2mmol)	0.0067g (0.02mmol)	330	8
2D shape: Six-pointed star, four-pointed star or regular triangle	0.0846g (0.25mmol)	0.09865g (0.25mmol)	0.0536g (0.4mmol)	0.0134g (0.04mmol)	650	12
3D shape: "3D-S-LCE",	0.0846g (0.25mmol)	0.09865g (0.25mmol)	0.0536g (0.4mmol)	0.0134g (0.04mmol)	650	12

Preprints (www.preprints.org) | NOT PEER-REVIEWED | Posted: 28 April 2023 doi:10.20944/preprints202304.1181.v1

"3D-E-LCE" or "3D-SE-LCE"	

2.2. Characterization methods

A polarizing optical microscope (POM, SMZ 1500, Nikon Instruments Co.) was used to determine the mesogenic alignment distributions in LCE matrices by measuring the transmittance of a probe light through a couple of crossed polarizer and analyzer with a LCE sample being set between them.

3. Results and discussion

The network of polysiloxane main-chain LCE was synthesized via a sol-gel processed hydrosilation [1, 75], as illustrated in Scheme 1. The precursor reactants included the monomers of mesogen "LC44" and "LC66", chain extender "EDDET" and crosslinker "PMPOPS". The terminal vinyl bonds of mesogenic molecules reacted with the Si-H bonds of chain extender molecules and crosslinker molecules under the action of platinic acid catalyst for hydrosilation polyaddition polymerization and crosslinking reaction to generate the LCE network. In the first step crosslinking, a partly crosslinked polydomain network, in which the mesogens were randomly oriented on average [1], was generated. Then an external force was applied to reshape it and establish a spatial alignment distribution of mesogens. After the second step crosslinking, the network topology with the mesogen alignments and the mechanically programmed material shape were permanently fixed. The preparation procedures of our LCEs with 1D, 2D or 3D programmed shapes were based on above principle, as described in Experiment Section, and "S-Ⅰ", "S-Ⅱ" and "S-Ⅲ" of the ESI†.

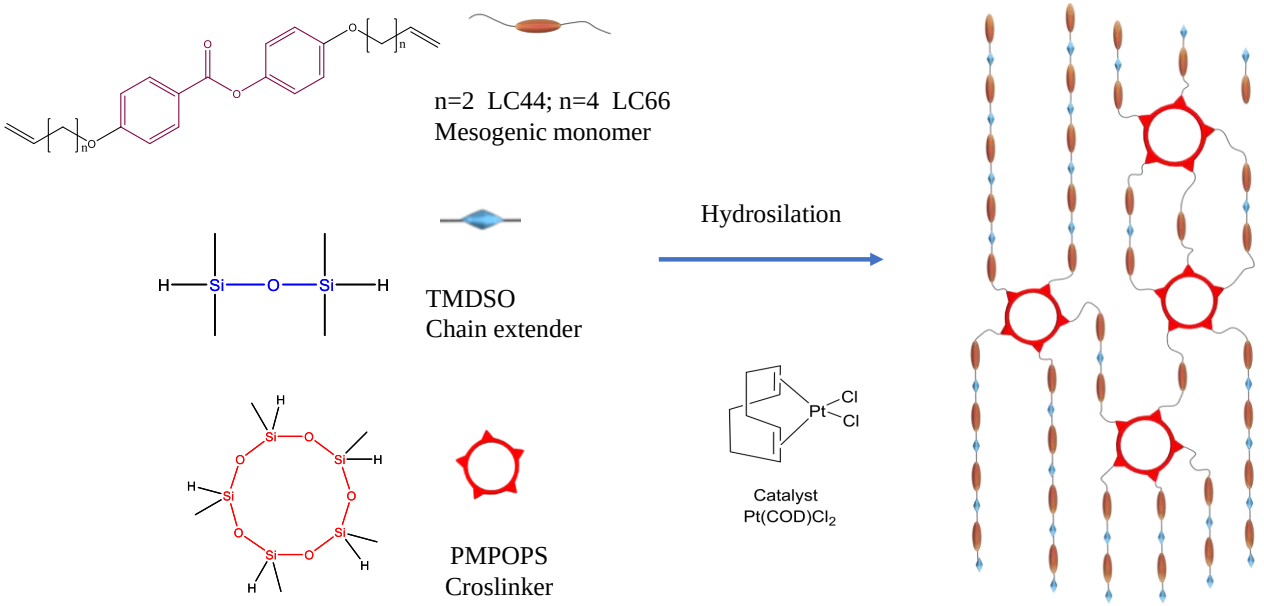

Scheme 1. Illustration of precursor reactant molecules and the synthesis of polysiloxane main-chain LCE network via hydrosilation reaction.

The two fabricated LCEs with 1D programmed shapes were in rectangular strip and round rod shape respectively, as expounded in "S-Ⅰ" of the ESI†. Figure 1(a) shows a POM observation of the strip-shaped LCE. The LCE exhibited brightest transmittance when its stretching direction was at an angle of ±45° with the polarizer or analyzer (Figure 1(a-Ⅰ, a-Ⅳ)), while extinctive transmittance was found when its stretching direction was parallel or perpendicular to the polarizer or analyzer (Figure 1(a-Ⅱ, a-III)), thus revealed that the mesogens were axially aligned along its stretching direction [1], as illustrated by Figure 1(b). The thermal-actuation behavior of strip-shaped LCE was examined on a

Preprints (www.preprints.org) | NOT PEER-REVIEWED | Posted: 28 April 2023 doi:10.20944/preprints202304.1181.v1

program-controlled hot stage, as shown in the photo-images of Figure 1(c). Upon heating to 80 ℃, it contracted along the length direction, which was the alignment direction, and expanded along the width direction. Upon cooling to room temperature, it returned to the initial length and width. This reversible thermal-induced deformation was caused by the reversible phase transition between the alignment structure and isotropic state upon the heating/cooling process [1-6]. When the LCE network transitioned from LC phase to isotropic state, it contracted along the alignment direction and expanded along the directions which were perpendicular to the alignment [1]. We found that the resulted dimensions in length and width of the rectangular strip-shaped LCE, under being heated above the T_{ni} (about 62 ℃ [75]), were basically consistent with those of the partly crosslinked polydomain LCE with rectangular strip shape after the first step crosslinking, as expounded in "S- Ⅰ" and illustrated in Scheme S1 of the ESI†. This revealed that the LCE demonstrated two-way shape memory between the initial shape formed after the first step crosslinking and the mechanically programmed shape which was fixed by the second step crosslinking. This two-way shape memory should be induced by the two-way network memory between the first network structure and the second network structure generated in the two-step crosslinking process [70].

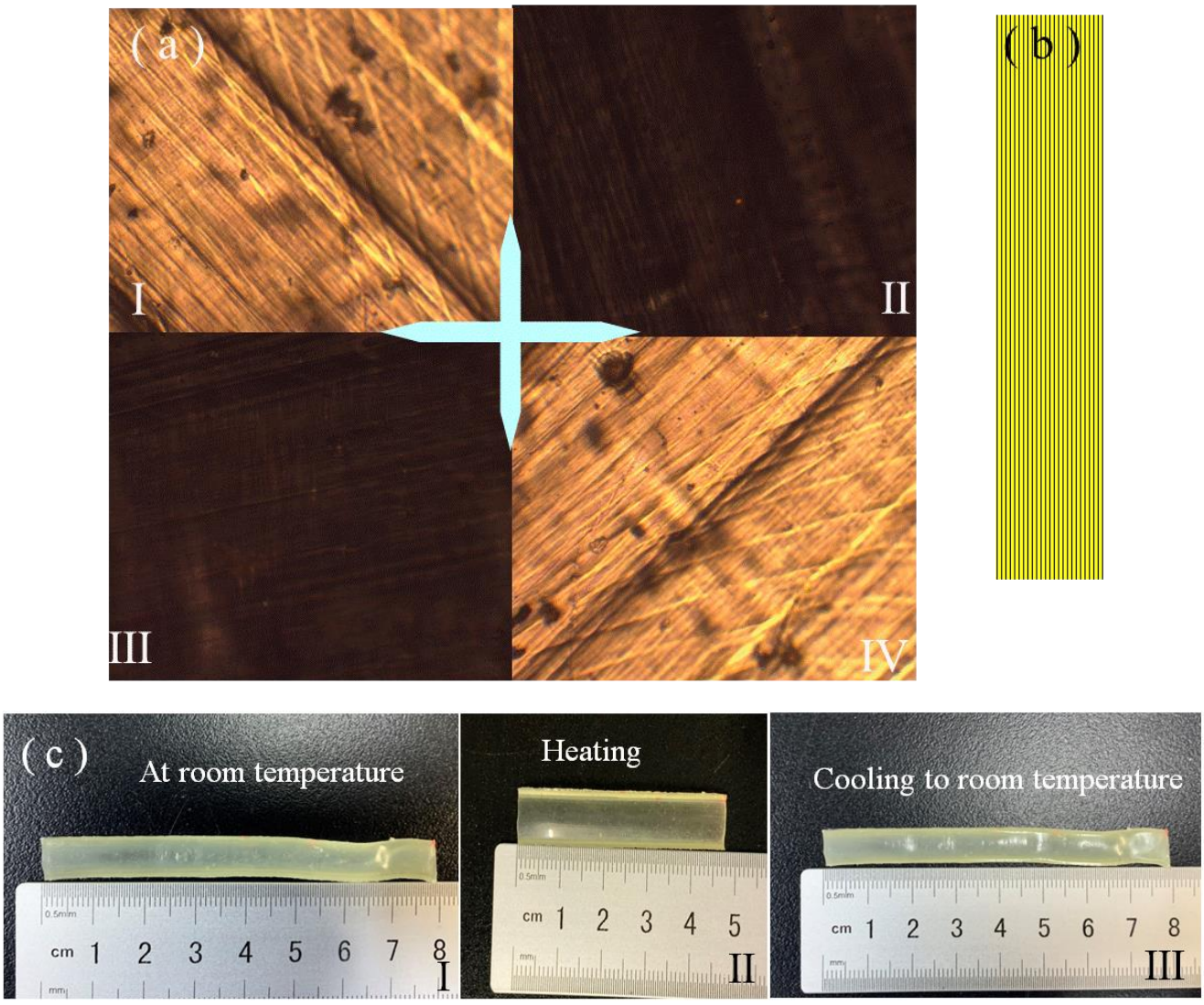

Figure 1. (a) POM images of the strip-shaped LCE. The crossed arrows denote the horizontal analyzer and vertical polarizer. (a-Ⅰ) The stretching direction inclined at -45° to the polarizer. (a-Ⅱ) The stretching direction paralleled to the polarizer. (a-Ⅲ) The stretching direction paralleled to the analyzer. (a-Ⅳ) The stretching direction inclined at 45° to the polarizer. (b) The schematic alignment

Preprints (www.preprints.org) | NOT PEER-REVIEWED | Posted: 28 April 2023 doi:10.20944/preprints202304.1181.v1

distribution in the strip-shaped LCE. (c) Photo-images of the states of strip-shaped LCE on a hot stage at room temperature initially (c-Ⅰ), being heated to 80 ℃ (c-Ⅱ) and being cooled to room temperature (c-Ⅲ).

A transversely cut slice of the rod-shaped LCE was used for POM measurement. As illustrated in Figure 2(a-Ⅰ), the coordinate locations marked as "1" to "9" were selected to be observed by POM. Coordinate locations "1" to "8" were near to the circumference edge, while coordinate location "9" was in center area. Coordinate locations "1" and "5" together located in a line which was parallel to the analyzer. Coordinate locations "3" and "7" together located in a line which was parallel to the polarizer. The line connecting with coordinate locations "2" and "6", and the line connecting with coordinate locations "4" and "8" were all at ±45° angle relative to the analyzer or polarizer. The POM images are shown in Figure 2(a-Ⅱ), the coordinate locations "1", "3", "5", "7" and "9" exhibited dark transmittance, while the coordinate locations "2", "4", "6" and "8" exhibited bright transmittance. The transmittance effects of these coordinate locations were constant after the cut slice was rotated by any angles. POM measurement evidenced that in the rod-shaped LCE, the mesogens were aligned along the radial directions in the area near to the circumference edge, but the center area was in disordered polydomain structure, as illustrated by Figure 2(a-Ⅲ). The photo-images shown in Figure 2(b) exhibited the thermal-actuation behavior of rod-shaped LCE on a program-controlled hot stage. Upon heating to 80 ℃, it elongated along the axial direction, and became a little thinner along the radial direction. Upon cooling to room temperature, it returned to initial axial and radial dimensions. This reversible shape changing mode upon the heating/cooling process also resulted from the alignment distribution. We found that the resulting dimensions in axial height and radial diameter of the rod-shaped LCE, under being heated to 80 ℃, were also basically consistent with those of the partly crosslinked polydomain LCE with rod shape after the first step crosslinking, as expounded in "S-Ⅰ" and illustrated in Scheme S2 of the ESI†. This revealed that the rod-shaped LCE also demonstrated two-way shape memory between the initial shape formed after the first step crosslinking and the mechanically programmed shape which was fixed by the second step crosslinking.

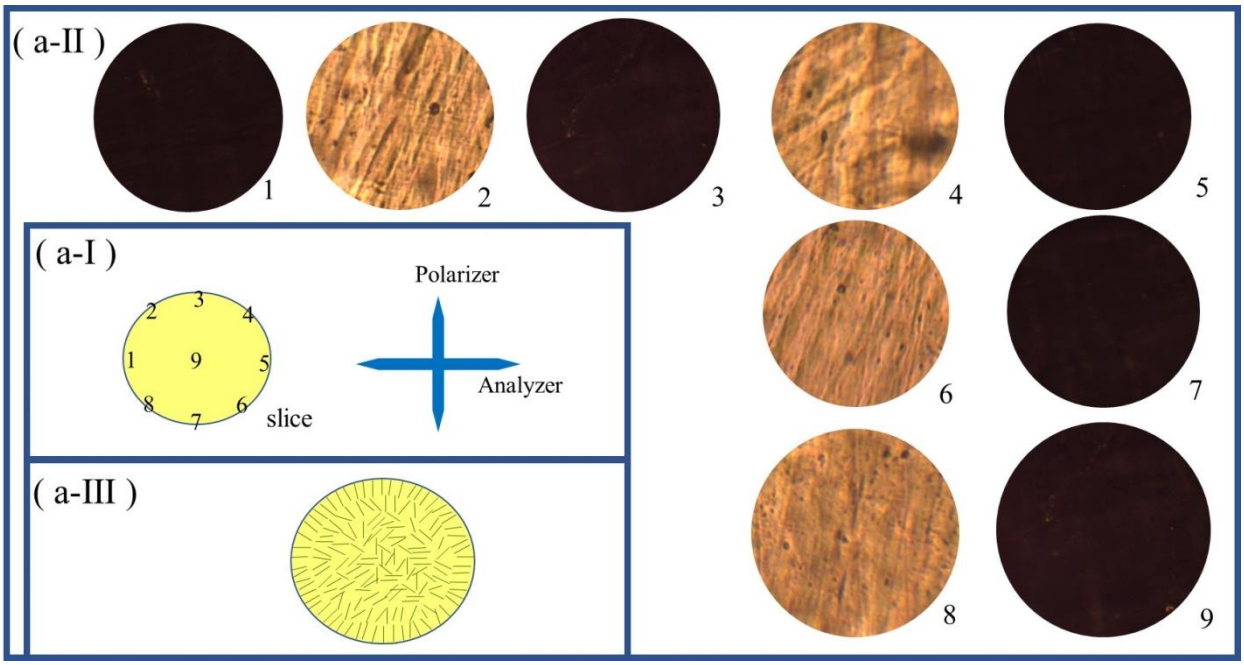

Preprints (www.preprints.org) | NOT PEER-REVIEWED | Posted: 28 April 2023 doi:10.20944/preprints202304.1181.v1

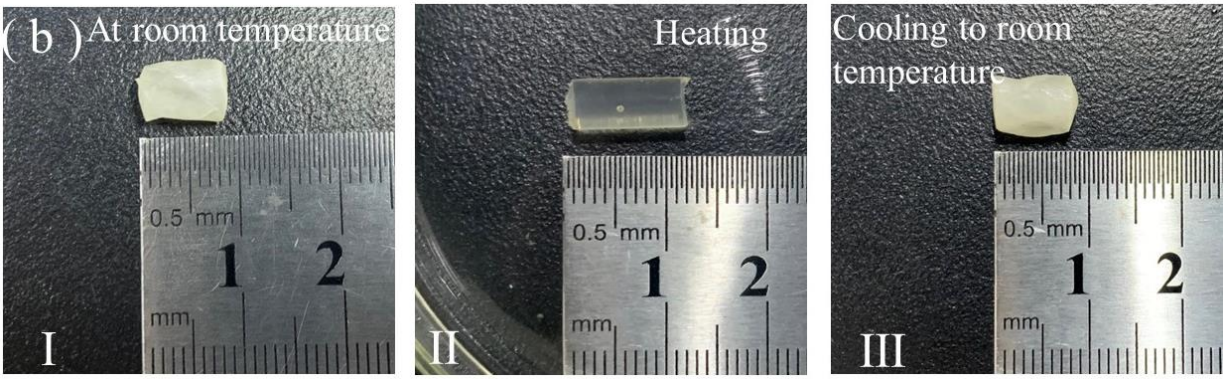

Figure 2. (a-Ⅰ) Schematic illustration of the selected coordinate locations, marked as "1" to "9", in a transversely cut silce of rod-shaped LCE, for POM measurement. The crossed arrows denote the horizontal analyzer and vertical polarizer. (a-Ⅱ) POM images captured at coordinate location "1" to "9". (a-Ⅲ) Schematic illustration of alignment distribution in cross section of the rod-shaped LCE. (b) Photo-images of the states of rod-shaped LCE on a hot stage at room temperature initially (b-Ⅰ), being heated to 80 ℃ (b-Ⅱ) and being cooled to room temperature (b-Ⅲ).

In order to qualify the two-way shape memory ability of our polysiloxane main-chain LCE materials, several parameters of actuation fixity for the 1D programmed LCEs were defined through leveraging the definition of actuation fixity parameters of SMP [71]. The defined actuation fixity parameters are cure fixity, "f_{cure}", heating deformation fixity, "f_{heat}", and cooling deformation fixity, "f_{cool}", as expounded in in "S-Ⅳ" of the ESI†. The measured actuation fixities of the strip-shaped LCE and rod-shaped LCE are listed in Table 2. It was indicated by Table 2 that actuation fixities were superior. Moreover, the measured values of "f_{heat}" and "f_{cool}" of 1D programmed LCEs were basically constant after several tens of repeated heating/cooling actuation. Thus, our polysiloxane main-chain LCE materials should be capable of effectively performing programmable complex shape morphings.

Table 2. The actuation fixities of 1D programmed LCEs.

Programmed shape	f_{cure}	f_{heat}	f_{cool}
Rectangular strip	98.1 %	98.8 %	≈100 %
Round rod	97.9 %	98.3 %	≈100 %

The three fabricated LCEs with 2D programmed shapes were in regular triangle shape, four-pointed star and six-pointed star respectively, as expounded in "S-Ⅱ" of the ESI†. The partly crosslinked polydomain LCE with disc shape, which was synthesized in first step crosslinking, was mechanically programmed to be an other shape of regular triangle, four-pointed star or six-pointed star, and then the programmed shape was fixed by the second step crosslinking, as shown in Scheme S3. As illustrated in Figure 3(a-Ⅰ), for a placed regular triangle-shaped LCE with one sideline being parallel to the analyzer, the coordinate locations marked as "1" to "11" were selected for POM observation. Coordinate location "1" located in the bisector of top angle, which was parallel to the polarizer, and near to the top angle. Coordinate locations "2" to "10" were respectively near to one sideline. Among them, coordinate locations "2", "3", "7", "8", "9" and "10" were respectively near to one angle, while coordinate locations "4", "5" and "6" were respectively near to the middle of one sideline. Coordinate location "11" located in center area of the regular triangle. The POM images are shown in Figure 3(a-Ⅱ), the coordinate locations "1", "6", "8", "10" and "11" exhibited dark transmittance, while the coordinate locations "2", "3", "4", "5", "7" and "9" exhibited bright transmittance. The transmittance effects of these coordinate locations were periodically consistent by cyclical rotating the sample with an interval angle of 120°. The alignment distribution in regular triangle-shaped LCE

 doi:10.20944/preprints202304.1181.v1

evidenced by POM measurement is shown in Figure 3(a-Ⅲ). In every angle, the alignments were symmetrically distributed with respect to the angular bisector. The alignments in the areas close to the angular bisectors were essentially parallel to them. The alignments in the middle part between any two angles were basically parallel to the sideline connecting the two angles. The center area of regular triangle-shaped LCE was in disordered polydomain structure. As illustrated in Figure 3(b-Ⅰ), for a placed four-pointed star-shaped LCE with the two diagonals being at ±45° angle relative to the analyzer or polarizer, the coordinate locations marked as "1" to "9" were selected for POM observation. Coordinate locations "1", "3", "5" and "7" were respectively near to one star tip. Coordinate locations "2", "4", "6" and "8" respectively located in one middle area between two adjacent star-blades. Coordinate location "9" located in center area of the four-pointed star. POM images are presented in Figure 3(b-Ⅱ), the coordinate locations "1", "3", "5" and "7" exhibited bright transmittance, while the coordinate locations "2", "4", "6", "8" and "9" exhibited dark transmittance. The transmittance effects of coordinate locations "1" to "8" were periodically consistent by cyclical rotating the sample with an interval angle of 90°. Coordinate location "9" kept dark transmittance at any rotation angle of the sample. The alignment distribution in four-pointed star-shaped LCE evidenced by POM measurement is shown in Figure 3(b-Ⅲ). In every star-blade, the alignments were symmetrically distributed with respect to the bisector. The alignments in the areas close to the bisectors were essentially parallel to them. The alignments in the middle area between every two adjacent star-blades were approximately parallel to the line connecting the two blade tips. The center area of four-pointed star-shaped LCE was in disordered polydomain structure. As illustrated in Figure 3(c-Ⅰ), for a placed six-pointed star-shaped LCE with one diagonal being parallel to the polarizer, the coordinate locations marked as "1" to "13" were selected for POM observation. Coordinate locations "1", "3", "5", "7", "9" and "11" were respectively near to one star tip. Coordinate locations "2", "4", "6", "8", "10" and "12" respectively located in one middle area between two adjacent star-blades. Coordinate location "13" located in center area of the six-pointed star. POM images presented in Figure 3(c-Ⅱ) indicate that the coordinate locations "1", "4", "7", "10" and "13" exhibited dark transmittance, while the coordinate locations "2", "3", "5", "6", "8", "9", "11" and "12" exhibited bright transmittance. The transmittance effects of these coordinate locations were periodically consistent by cyclical rotating the sample with an interval angle of 60°. The alignment distribution in six-pointed star-shaped LCE evidenced by POM measurement is shown in Figure 3(c-Ⅲ). In every star-blade, the alignments were symmetrically distributed with respect to the bisector. The alignments in the areas close to the bisectors were essentially parallel to them. The alignments in the middle area between every two adjacent star-blades were approximately parallel to the line connecting the two blade tips. The center area of six-pointed star-shaped LCE was in disordered polydomain structure.

Preprints (www.preprints.org) | NOT PEER-REVIEWED | Posted: 28 April 2023 doi:10.20944/preprints202304.1181.v1

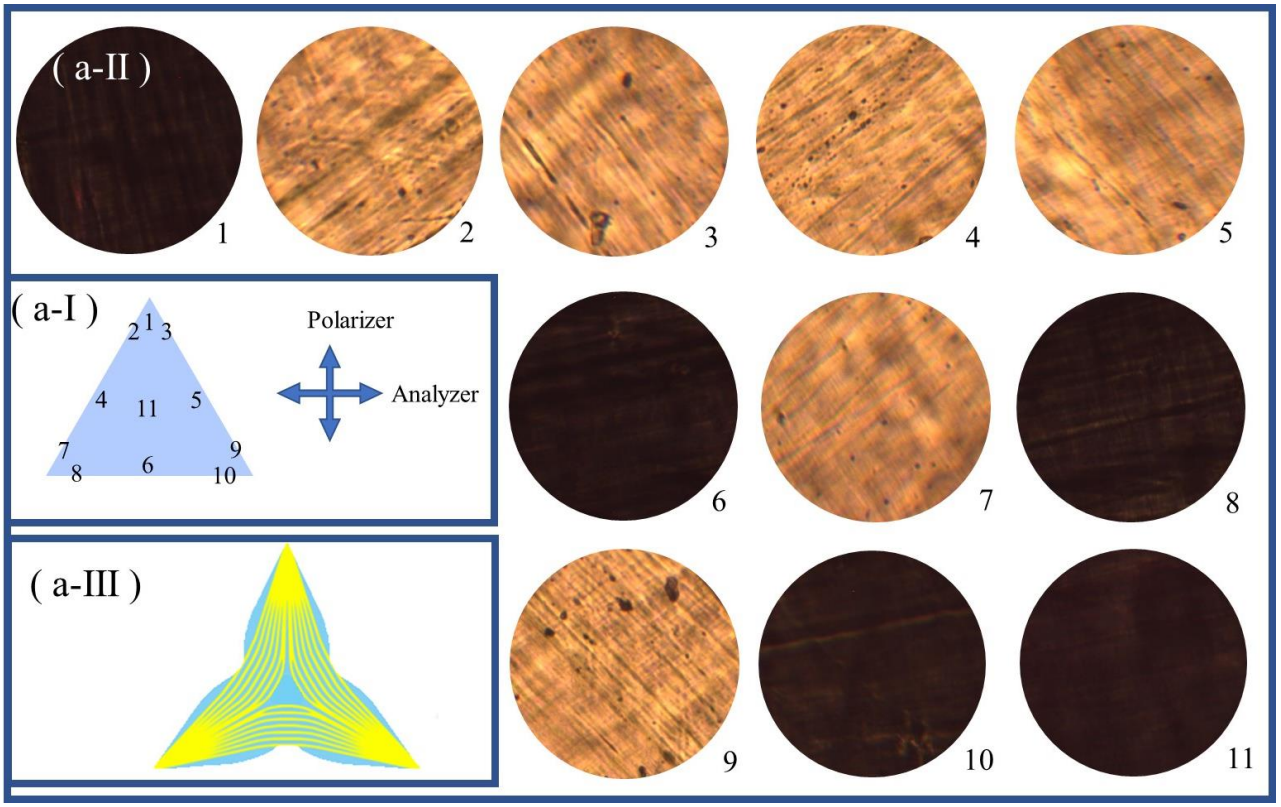

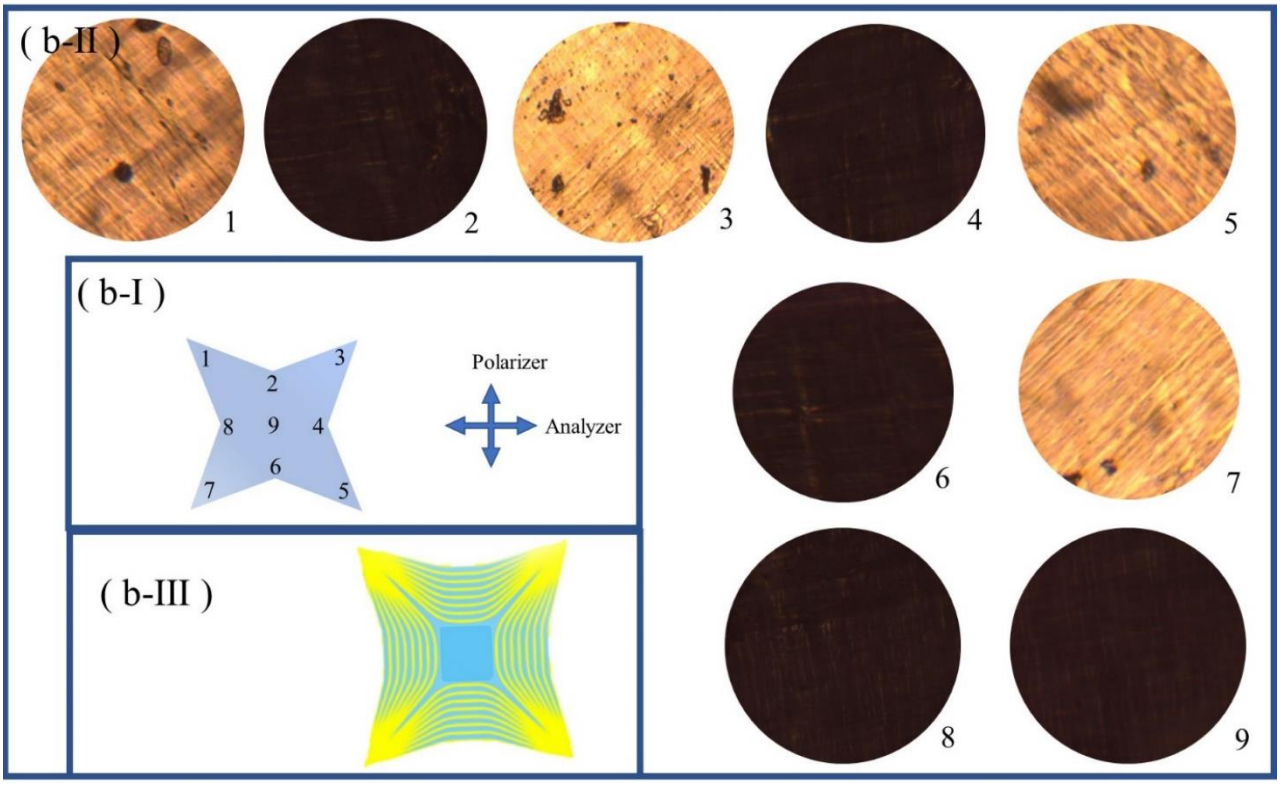

Preprints (www.preprints.org) | NOT PEER-REVIEWED | Posted: 28 April 2023 doi:10.20944/preprints202304.1181.v1

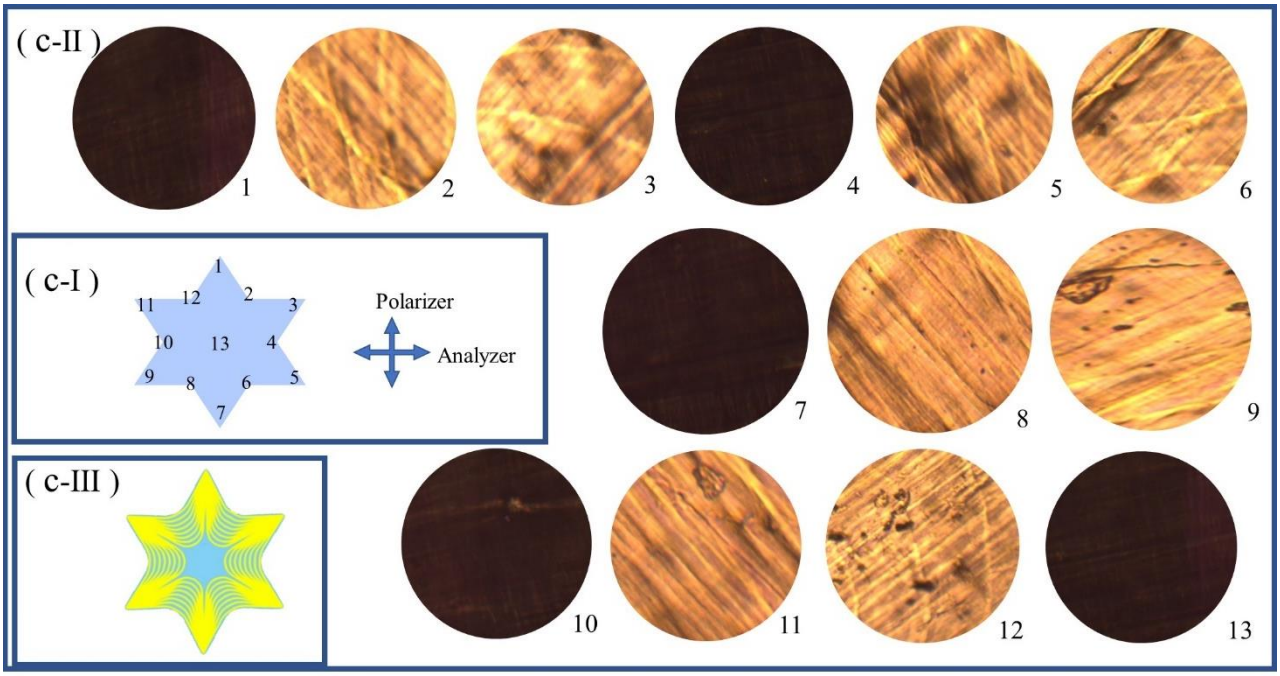

Figure 3. (a-Ⅰ, b-Ⅰ, c-Ⅰ) Schematic illustration of the selected coordinate locations, with number marking, in the LCE sample with a shape of regular triangle (a-Ⅰ), four-pointed star (b-Ⅰ) or six-pointed star (c-Ⅰ) for POM measurement. The crossed arrows denote the horizontal analyzer and vertical polarizer. (a-Ⅱ, b-Ⅱ, c-Ⅱ) POM images captured at the selected coordinate locations of regular triangle shaped LCE (a-Ⅱ), four-pointed star-shaped LCE (b-Ⅱ) and six-pointed star shaped LCE (c-Ⅱ). (a-Ⅲ, b-Ⅲ, c-Ⅲ) Schematic illustrations of alignment distributions in regular triangle shaped LCE (a-Ⅲ), four-pointed star-shaped LCE (b-Ⅲ) and six-pointed star-shaped LCE (c-Ⅲ).

The thermal-actuation behaviors of the regular triangle shaped LCE, four-pointed star shaped LCE and six-pointed star shaped LCE were examined on a program-controlled hot stage. As shown in Figure 4, Moive S1, S2 and S3 of the ESI†, upon heating to 80 ℃, the regular triangle shaped LCE, four-pointed star shaped LCE and six-pointed star shaped LCE all changed to be disc shape, whose shape and diameter were consistent with the partly crosslinked polydomain LCEs synthesized in first step crosslinking. Upon cooling to room temperature, they resumed their respective shapes and dimensions. These LCEs with 2D programmed shapes all demonstrated well two-way shape memory performance though their geometries and mesogen alignment distributions were different.

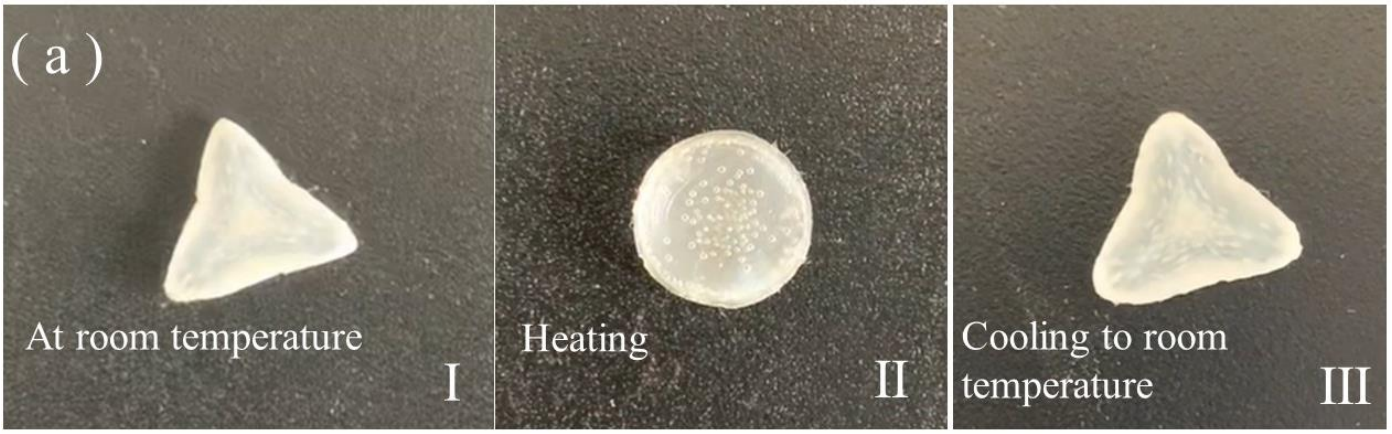

Preprints (www.preprints.org) | NOT PEER-REVIEWED | Posted: 28 April 2023 doi:10.20944/preprints202304.1181.v1

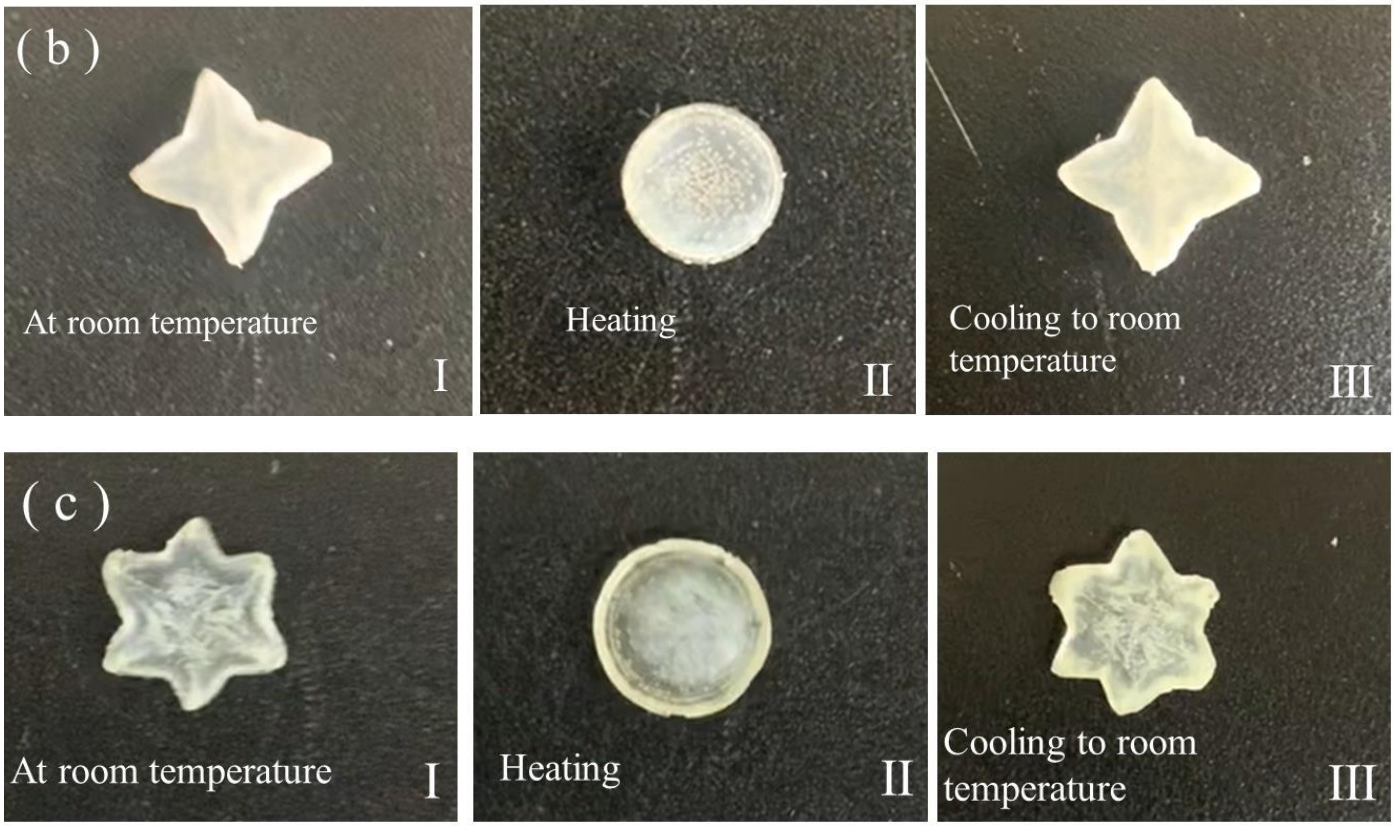

Figure 4. Photo-images of the states of regular triangle shaped LCE (c), four-star shaped LCE (b) and six-pointed star-shaped LCE (c) on a hot stage at room temperature initially (a-Ⅰ, b-Ⅰ, c-Ⅰ), being heated to 80 ℃ (a-Ⅱ, b-Ⅱ, c-Ⅱ) and being cooled to room temperature (a-Ⅲ, b-Ⅲ, c-Ⅲ).

The fabrications of three LCEs with 3D programmed shapes, which were nominated as "3D-S-LCE", "3D-E-LCE" and "3D-SE-LCE" respectively, are expounded in "S-Ⅲ" of the ESI†. For the fabrication of "3D-S-LCE", the partly crosslinked polydomain LCE synthesized in first step crosslinking was in disc shape with a 3D pattern of Heilongjiang university logo on one surface, which was stamped by a badge during the first step crosslinking. The patterned surface was mechanically pressed to be flat. Then the flattened surface was fixed by the second step crosslinking, as shown in Scheme S4. For the fabrication of "3D-E-LCE", the partly crosslinked polydomain LCE synthesized in first step crosslinking was in disc shape with flat surfaces. A 3D plum blossom was mechanically embossed on its one surface by a plum blossom plastic mould (No.1 plastic mould) and then fixed by the second step crosslinking, as shown in Scheme S5. For the fabrication of "3D-SE-LCE", the partly crosslinked polydomain LCE synthesized in first step crosslinking had a stamped 3D pattern of Heilongjiang university logo on one surface. The patterned surface was mechanically embossed to be another 3D plum blossom shape by another plum blossom plastic mould (No.2 plastic mould) and then fixed by the second step crosslinking, as shown in Scheme S6. The thermal-actuation behaviors of "3D-S-LCE", "3D-E-LCE" and "3D-SE-LCE" were examined on a program-controlled hot stage, as shown in Figure 5, Moive S4, S5 and S6 of the ESI†. For the "3D-S-LCE", the initial stamped 3D pattern of Heilongjiang university logo formed in first step crosslinking re-appeared on its surface when it was heated to 80 ℃. Upon cooling to room temperature, the surface resumed flatness state. For the "3D-E-LCE", upon heating to 80 ℃, the 3D plum blossom disappeared and the surface became flat. Upon cooling to room temperature, the surface resumed its 3D plum blossom pattern. For the "3D-SE-LCE", the 3D plum blossom pattern on its surface changed to be the 3D pattern of Heilongjiang university logo formed in first step crosslinking. Upon cooling to room temperature, the surface changed back to 3D plum blossom pattern. The fabricated LCEs with 3D programmed shapes had complicated

Preprints (www.preprints.org) | NOT PEER-REVIEWED | Posted: 28 April 2023 doi:10.20944/preprints202304.1181.v1

topological structures and spatial distributions of mesogen alignments which were difficult to be clearly measured. Therefore, it is very hard to foresight their shape changing modes by mean of determining the LC orientation profiles. However, by using the capability of two-way shape memory, reversible shape morphings between arbitrary complicated 3D shapes predetermined by mechanical shaping procedures can be conveniently programmed and achieved.

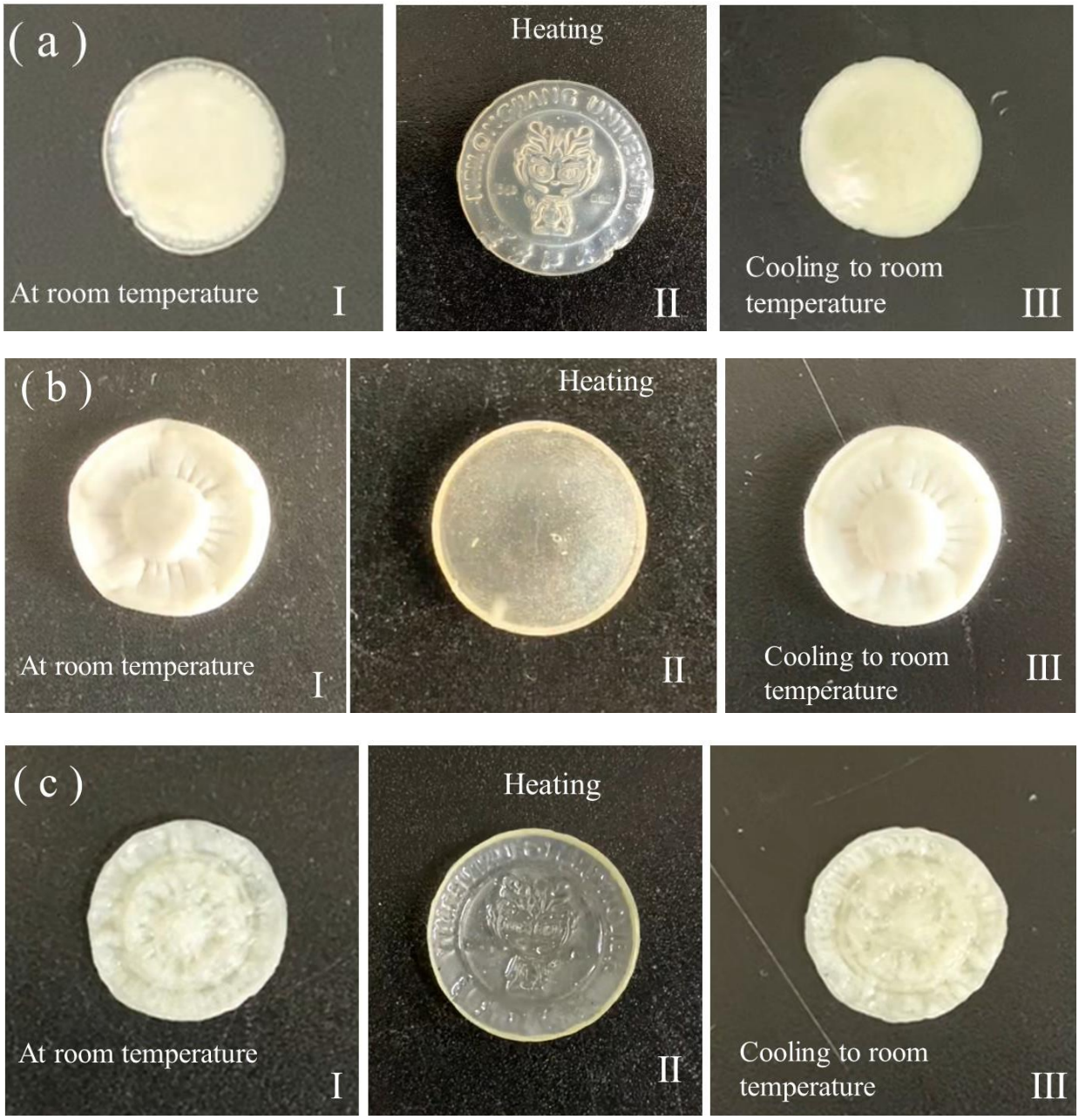

Figure 5. Photo-images of the states of "3D-S-LCE" (a), "3D-E-LCE" (b) and "3D-SE-LCE" (c) on a hot stage at room temperature initially (a-Ⅰ, b-Ⅰ, c-Ⅰ), being heated to 80 ℃ (a-Ⅱ, b-Ⅱ, c-Ⅱ) and being cooled to room temperature (a-Ⅲ, b-Ⅲ, c-Ⅲ).

4. Conclusions

To sum up, we presented the result of direct programming complex reversible shape morphing in polysiloxane main-chain LCEs by using mechanical programming process, which was inspired by the principle of using "mechanical programming process" to achieve programmable shape changing behavior in SMPs. In the approach, polydomain LCEs were first synthesized with distinct geometries, which were not limited to flat

shapes, via a sol-gel processed hydrosilation reaction. The programmed arbitrary shaped LCEs were prepared by mechanical programming, such as stretching, pressing, stamping or embossing, the polydomain LCEs and subsequent the second crosslinking step. After second crosslinking to permanently fix the programmed LCE shape and the alignment distribution of mesogens formed by mechanical programming process, the resulting LCEs exhibited reversible shape morphing between the initial and programmed shapes, which were induced by the LC phase transition, upon heating and cooling process. This facile and versatile strategy of realizing programmable shape morphing performance utilized the property of two-way memory between the first network structure and the second network structure generated in the two-step crosslinking process, and thus jumped out of the suffering of meticulous modulating the spatial distribution of mesogen alignments. This strategy is suitable for polysiloxane main-chain LCEs due to their well processability, elasticity, and well reactivity during preparation, which made them to be easily fabricated into different initial shapes, and programmed into various complex shapes. Our work should widen the prospect for the design and application of LCE materials in smart actuators, biomedical devices, soft robotics and multi-functional structures, *etc*, where arbitrary and easily programmed shape morphings are needed.

Supplementary Materials: Electronic supplementary information (ESI) available**:** Supplementary movie S1: Movie of thermal induced programmable shape change of the LCE with a geometry of regular triangle. speed: 3×; Supplementary movie S2: Movie of thermal induced programmable shape change of the LCE with a geometry of four-pointed star. speed: 3×; Supplementary movie S3: Movie of thermal induced programmable shape change of the LCE with a geometry of six-pointed star. speed: 3×; Supplementary movie S4: Movie of thermal induced programmable shape change of the "3D-S-LCE". speed: 3×; Supplementary movie S5: Movie of thermal induced programmable shape change of the "3D-E-LCE". speed: 3×; Supplementary movie S6: Movie of thermal induced programmable shape change of the "3D-SE-LCE". speed: 3×.

Acknowledgments: We acknowledge the funding support from the Natural Science Foundation of Heilongjiang Province of China through the Grant No. LH2020E106, and the Open Research Fund Program of Institute of regulatory science of Beijing Technology and Business University through the Grant No. CRS-2020-01. We also acknowledge the academic discussion and technical support given by the researchers in the Chemistry Department and Chemical engineering Department of Heilongjiang University.

Conflicts of interest: There are no conflicts to declare

References

1. De Jeu, W. H. *Liquid Crystal Elastomers: Materials and Applications.* Aachen University, Aachen, Germany, 2012**.**
2. Pilz da Cunha, M.; Debije, M. G.; Schenning, A. P. H. J. Bioinspired light-driven soft robots based on liquid crystal polymers. *Chem. Soc. Rev.* **2020**, *49*, 6568-6578.
3. Wang, Q. E.; Niu, H.; Wang, Y.; Li, C. Carbon nanotubes modified nanocomposites based on liquid crystalline elastomers. *Mol. Cryst. Liq. Cryst.* **2021**, *732*, 11-49.
4. Schwartz, M.; Lagerwall, J. P. F. Embedding intelligence in materials for responsive built environment: A topical review on Liquid Crystal Elastomer actuators and sensors. *Build. Environ.* **2022**, *226*, 109714.
5. Wang, Y. C.; Liu, J. Q.; Yang, S. Multi-functional liquid crystal elastomer composites. *Appl. Phys. Rev.* **2022**, *9*, 011301.
6. Zhang, W.; Nan, Y. F.; Wu, Z. X.; Shen, Y. J.; Luo, D. Photothermal-Driven Liquid Crystal Elastomers: Materials, Alignment and Applications. *Molecules* **2022**, *27*, 4330.
7. Liu, L.; Wang, M.; Guo, L.-X.; Sun, Y.; Zhang, X.-Q.; Lin, B.-P.; Yang, H. Aggregation-Induced Emission Luminogen-Functionalized Liquid Crystal Elastomer Soft Actuators. *Macromolecules* **2018**, *51*, 4516-4524.
8. Saed, M. O.; Ambulo, C. P.; Kim, H.; De, R.; Raval, V.; Searles, K.; Siddiqui, D. A.; Cue, J. M. O.; Stefan, M. C.; Shankar, M. R.; Ware, T. H. Molecularly-Engineered, 4D-Printed Liquid Crystal Elastomer Actuators. *Adv. Funct. Mater.***2019**, *29*, 1806412.
9. Chen, Q.; Li, Y.; Yang, Y.; Xu, Y.; Qian, X.; Wei, Y.; Ji, Y. Durable liquid-crystalline vitrimer actuators. *Chem. Sci.* **2019**, *10*, 3025-3030.
10. Zuo, B.; Wang, M.; Lin, B. P.; Yang, H. Visible and infrared three-wavelength modulated multi-directional actuators. *Nat. Commun.* **2019**, *10*, 4539.
11. He, Q.; Wang, Z.; Wang, Y.; Song, Z.; Cai, S. Recyclable and Self-Repairable Fluid-Driven Liquid Crystal Elastomer Actuator. *ACS Appl. Mater. Interfaces* **2020**, *12*, 35464-35474.

12. Li, Y.; Liu, Y.; Luo, D. Polarization Dependent Light-Driven Liquid Crystal Elastomer Actuators Based on Photothermal Effect. *Adv. Opt. Mater.* **2020**, *9*, 2001861.1-2001861.9.
13. Xu, J.; Zhao, N.; Qin, B.; Qu, M.; Wang, X.; Ridi, B.; Li, C.; Gao, Y. Optical Wavelength Selective Photoactuation of Nanometal-Doped Liquid Crystalline Elastomers by Using Surface Plasmon Resonance. *ACS Appl. Mater. Interfaces* **2021**, *13*, 44833-44843.
14. Yao, L. R.; Yan, H. X.; He, Y. F.; Zhao, N.; Wang, X. X.; Li, C. S.; Sun, L. G.; He, Y.; Liu, Y. J.; Zhang, J. Q. Actuation performances of catkin fibers reinforced thiol-acrylate main-chain liquid crystalline elastomer. *Int. J. Smart Nano Mat.* **2022**, *13*, 668-690.
15. Zhang, X.Y.; Yao, L. R.; Yan, H. X.; Zhang, Y. H.; Han, D. X.; He, Y. F.; Li, C. S.; Zhang, J. Q. Optical wavelength selective actuation of dye doped liquid crystalline elastomers by quasi-daylight. *Soft Matter* **2022**, *18*, 9181-9196.
16. Zhao, T.; Zhang, Y.; Fan, Y.; Wang, J.; Jiang, H.; Lv, J.-A. Light-modulated liquid crystal elastomer actuator with multimodal shape morphing and multifunction. *J. Mater. Chem. C.* **2022**, *10*, 3796-3803.
17. Qian, X.; Chen, Q.; Yang, Y.; Xu, Y.; Li, Z.; Wang, Z.; Wu, Y.; Wei, Y.; Ji, Y. Untethered Recyclable Tubular Actuators with Versatile Locomotion for Soft Continuum Robots. *Adv. Mater.* **2018**, *30*, 1801103.
18. Zeng, H.; Wasylczyk, P.; Wiersma, D. S.; Priimagi, A. Light Robots: Bridging the Gap between Microrobotics and Photomechanics in Soft Materials. *Adv. Mater.* **2018**, *30*, 1703554.
19. He, Q. G.; Wang, Z. J.; Wang, Y.; Minori, A.; Tolley, M. T.; Cai, S. Q. Electrically controlled liquid crystal elastomer-based soft tubular actuator with multimodal actuation. *Sci. Adv.* **2019**, *5*, eaax5746.
20. Shen, C.; Lan, R.; Huang, R.; Zhang, Z.; Bao, J.; Zhang, L.; Yang, H. Photochemically and Photothermally Controllable Liquid Crystalline Network and Soft Walkers. *ACS App. Mater. Interfaces* **2021**, *13*, 3221-3227.
21. Li, Y.; Yu, H. B.; Yu, K.; Guo, X. G.; Wang, X. J. Reconfigurable Three-Dimensional Mesotructures of Spatially Programmed Liquid Crystal Elastomers and Their Ferromagnetic Composites. *Adv. Funct. Mater.* **2021**, *31*, 2100338.
22. Zhang, J.; Guo, Y.; Hu, W.; Soon, R. H.; Davidson, Z. S.; Sitti, M. Liquid Crystal Elastomer-Based Magnetic Composite Films for Reconfigurable Shape-Morphing Soft Miniature Machines. *Adv. Mater.* **2021**, *33*, 2006191.
23. Apsite, I.; Salehi, S.; Ionov, L. Materials for Smart Soft Actuator Systems. *Chem. Rev.* **2022**, *122*, 1349-1415.
24. Yu, Z.; Wang, Y.; Zheng, J.; Sun, S.; Fu, Y.; Chen, D.; Cai, W.; Wang, D.; Zhou, H.; Li, D. Fast-Response Bioinspired Near-Infrared Light-Driven Soft Robot Based on Two-Stage Deformation. *ACS Appl. Mater. Interfaces* **2022**, *14*, 16649-16657.
25. Tian, H.; Wang, Z.; Chen, Y.; Shao, J.; Gao, T.; Cai, S. Polydopamine-Coated Main-Chain Liquid Crystal Elastomer as Optically Driven Artificial Muscle. *ACS Appl. Mater. Interfaces* **2018**, *10*, 8307-8316.
26. Kim, H.; Lee, J. A.; Ambulo, C. P.; Lee, H. B.; Kim, S. H.; Naik, V. V.; Haines, C. S.; Aliev, A. E.; Ovalle-Robles, R.; Baughman, R. H.; Ware, T. H. Intelligently Actuating Liquid Crystal Elastomer-Carbon Nanotube Composites. *Adv. Funct. Mater.* **2019**, *29*, 1905063.
27. Lu, H.-F.; Wang, M.; Chen, X.-M.; Lin, B.-P.; Yang, H. Interpenetrating Liquid-Crystal Polyurethane/Polyacrylate Elastomer with Ultrastrong Mechanical Property. *J. Am. Chem. Soc.* **2019**, *141*, 14364-14369.
28. Roach, D. J.; Yuan, C.; Kuang, X.; Li, V. C.-F.; Blake, P.; Romero, M. L.; Hammel, I.; Yu, K.; Qi, H. J. Long Liquid Crystal Elastomer Fibers with Large Reversible Actuation Strains for Smart Textiles and Artificial Muscles. *ACS Appl. Mater. Interfaces* **2019**, *11*, 19514-19521.
29. Liu, H.; Tian, H.; Shao, J.; Wang, Z.; Li, X.; Wang, C.; Chen, X. An Electrically Actuated Soft Artificial Muscle Based on a High-Performance Flexible Electrothermal Film and Liquid-Crystal Elastomer. *ACS Appl. Mater. Interfaces* **2020**, *12*, 56338-56349.
30. Chen, C.; Liu, Y.; He, X.; Li, H., Chen, Y.; Wei, Y.; Zhao, Y.; Ma, Y.; Chen, Z.; Zheng, X.; Liu, H. Multiresponse Shape-Memory Nanocomposite with a Reversible Cycle for Powerful Artificial Muscles. *Chem. Mater.* **2021**, *33*, 987-997.
31. Lee, J. H.; Bae, J.; Hwang, J. H.; Choi, M. Y.; Kim, Y. S.; Park, S.; Na, J. H.; Kim, D. G.; Ahn, S. K. Robust and Reprocessable Artificial Muscles Based on Liquid Crystal Elastomers with Dynamic Thiourea Bonds. *Adv. Funct. Mater.* **2022**, *32*, 2110360.
32. Zhao, N.; Wang, X.; Yao, L.; Yan, H.; Qin, B.; Li, C.; Zhang, J. Actuation performance of a liquid crystalline elastomer composite reinforced by eiderdown fibers. *Soft Matter* **2022**, *18*, 1264-1274.
33. Lv, J. A.; Liu, Y. Y.; Wei, J.; Chen, E. Q.; Qin, L.; Yu, Y. L. Photocontrol of fluid slugs in liquid crystal polymer microactuators. *Nature* **2016**, *537*, 179.
34. Palagi, S.; Mark, A. G.; Reigh, S. Y.; Melde, K.; Qiu, T.; Zeng, H.; Parmeggiani, C.; Martella, D.; Sanchez-Castillo, A.; Kapernaum, N.; Giesselmann, F.; Wiersma, D. S.; Lauga, E.; Fischer, P. Structured light enables biomimetic swimming and versatile locomotion of photoresponsive soft microrobots. *Nat. Mater.* **2016**, *15*, 647.
35. Wang, M.; Lin, B. P.; Yang, H. A plant tendril mimic soft actuator with phototunable bending and chiral twisting motion modes. *Nat. Commun.* **2016**, *7*, 13981.
36. Shahsavan, H.; Salili, S. M.; Jakli, A.; Zhao, B. Thermally Active Liquid Crystal Network Gripper Mimicking the Self-Peeling of Gecko Toe Pads. *Adv. Mater.* **2017**, *29*, 1604021.
37. Zuo, B.; Wang, M.; Lin, B.-P.; Yang, H. Photomodulated Tricolor-Changing Artificial Flowers. *Chem. Mater.* **2018**, *30*, 8079-8088.
38. Ferrantini, C.; Pioner, J. M.; Martella, D.; Coppini, R.; Piroddi, N.; Paoli, P.; Calamai, M.; Pavone, F. S.; Wiersma, D. S.; Tesi, C.; Cerbai, E.; Poggesi, C.; Sacconi, L.; Parmeggiani, C. Development of Light-Responsive Liquid Crystalline Elastomers to Assist Cardiac Contraction. *Circ. Res.* **2019**, *124*, e44-e54.

39. Shaha, R. K.; Merkel, D. R.; Anderson, M. P.; Devereaux, E. J.; Patel, R. R.; Torbati, A. H.; Willett, N.; Yakacki, C. M.; Frick, C. P. Biocompatible liquid-crystal elastomers mimic the intervertebral disc. *J. Mech. Behav. Biomed. Mater.* **2020**, *107*, 103757.
40. Hussain, M.; Jull, E. I. L.; Mandle, R. J.; Raistrick, T.; Hine, P. J.; Gleeson, H. F. Liquid Crystal Elastomers for Biological Applications. *Nanomaterials* **2021**, *11*, 813.
41. Liu, Z.; Bisoyi, H. K.; Huang, Y.; Wang, M.; Yang, H.; Li, Q. Thermo- and Mechanochromic Camouflage and Self-Healing in Biomimetic Soft Actuators Based on Liquid Crystal Elastomers. *Angew. Chem. Int. Ed.* **2022**, *61*, e202115755.
42. Wang, Y. P.; Liao, W.; Sun, J. H.; Nandi, R.; Yang, Z. Q. Bioinspired Construction of Artificial Cardiac Muscles Based on Liquid Crystal Elastomer Fibers. *Adv. Mater. Technol.* **2022**, *7*, 2100934.
43. Wie, J. J.; Lee, K.; Smith, M. L.; Vaia, R. A.; White, T. J. Torsional mechanical responses in azobenzene functionalized liquid crystalline polymer networks. *Soft Matter* **2013**, *9*, 9303-9310.
44. Iamsaard, S.; Abhoff, S. J.; Matt, B.; Kudernac, T.; Cornelissen, J. L. M.; Fletcher, S. P.; Katsonis, N. Conversion of light into macroscopic helical motion. *Nat. Chem.* **2014**, *6*, 229-235.
45. Ware, T. H.; McConney, M. E.; Wie, J. J.; Tondiglia, V. P.; White, T. J. Voxelated liquid crystal elastomers. *Science* **2015**, *347*, 982-984.
46. Donovan, B. R.; Matavulj, V. M.; Ahn, S.-K.; Guin, T.; White, T. J. All-Optical Control of Shape. *Adv. Mater.* **2019**, *31*, 1805750.
47. Herbert, K. M.; Fowler, H. E.; McCracken, J. M.; Joselle, M.; Schlafmann, K. R.; Kyle, R.; Koch, J. A.; White, T. J. Synthesis and alignment of liquid crystalline elastomers. *Nat. Rev. Mater.* **2022**, *7*, 23-38.
48. Ohm, C.; Serra, C.; Zentel, R. A Continuous Flow Synthesis of Micrometer-Sized Actuators from Liquid Crystalline Elastomers. *Adv. Mater.* **2009**, *21*, 4859-4862.
49. Ohm, C.; Kapernaum, N.; Nonnenmacher, D.; Giesselmann, F.; Serra, C.; Zentel, R. Microfluidic Synthesis of Highly Shape-Anisotropic Particles from Liquid Crystalline Elastomers with Defined Director Field Configurations. *J. Am. Chem. Soc.* **2011**, *133*, 5305-5311.
50. Fleischmann, E.-K.; Liang, H.-L.; Kapernaum, N.; Giesselmann, F.; Lagerwall, J.; Zentel, R. One-piece micropumps from liquid crystalline core-shell particles. *Nat. Commun.* **2012**, *3*, 1178-1185.
51. Yaroshchuk, O.; Reznikov, Y. Photoalignment of liquid crystals: basics and current trends. *J. Mater. Chem.* **2012**, *22*, 286-300.
52. Ware, T. H.; Biggins, J. S.; Shick, A. F.; Warner, M.; White, T. J. Localized soft elasticity in liquid crystal elastomers. *Nat. Commun.* **2016**, *7*, 10781.
53. Zhao, J. Y.; Zhang, L. M.; Hu, J. Varied Alignment Methods and Versatile Actuations for Liquid Crystal Elastomers: A Review. *Adv. Intell. Syst.* **2022**, *4*, 2100065.
54. Buguin, A.; Li, M.-H.; Silberzan, P.; Ladoux, B.; Keller, P. Micro-actuators: when artificial muscles made of nematic liquid crystal elastomers meet soft lithography. *J. Am. Chem. Soc.* **2006**, *128*, 1088-1089.
55. Yang, H.; Buguin, A.; Taulemesse, J.-M.; Kaneko, K.; Mery, S.; Bergeret, A.; Keller, P. Micron-Sized Main-Chain Liquid Crystalline Elastomer Actuators with Ultralarge Amplitude Contractions. *J. Am. Chem. Soc.* **2009**, *131*, 15000-15004.
56. Cui, J.; Drotlef, D. M.; Larraza, I.; Ferna´ndez-Bla´zquez, J. P.; Boesel, L. F.; Ohm, C.; Mezger, M.; Zentel, R.; del Campo, A. Bioinspired Actuated Adhesive Patterns of Liquid Crystalline Elastomers. *Adv. Mater.* **2012**, *24*, 4601-4604.
57. Ambulo, C.; Burroughs, J. J.; Boothby, J. M.; Kim, H.; Shankar, M. R.; Ware, T. H. Four-dimensional Printing of Liquid Crystal Elastomers. *ACS Appl. Mater. Interfaces* **2017**, *9*, 37332-37339.
58. Lo´pez-Valdeolivas, M.; Liu, D.; Broer, D. J.; Sa´nchezSomolinos, C. 4D Printed Actuators with Soft-Robotic Functions. *Macromol. Rapid Commun.* **2018**, *39*, 1700710.
59. Kotikian, A.; Truby, R. L.; Boley, J. W.; White, T. J.; Lewis, J. A. 3D Printing of Liquid Crystal Elastomeric Actuators with Spatially Programed Nematic Order. *Adv. Mater.* **2018**, *30*, 1706164.
60. Wang, Z. J.; Guo, Y. B.; Cai, S. Q.; Yang, J. P. Three-Dimensional Printing of Liquid Crystal Elastomers and Their Applications. *ACS Appl. Polym. Mater.* **2022**, *4*, 3153-3168.
61. Wang, Y. P.; An, J.; Lee, H. Recent advances in molecular programming of liquid crystal elastomers with additive manufacturing for 4D printing. *Mol. Syst. Des. Eng.* **2022**, *7*, 1588-1601.
62. Pei, Z.; Yang, Y.; Chen, Q.; Terentjev, E. M.; Wei, Y.; Ji, Y. Mouldable liquid-crystalline elastomer actuators with exchangeable covalent bonds. *Nat. Mater.* **2014**, *13*, 36-41.
63. Pei, Z.; Yang, Y.; Chen, Q.; Wei, Y.; Ji, Y. Regional Shape Control of Strategically Assembled Multishape Memory Vitrimers. *Adv. Mater.* **2016**, *28*, 156-160.
64. McBride, M. K.; Hendrikx, M.; Liu, D.; Worrell, B. T.; Broer, D. J.; Bowman, C. N. Photoinduced Plasticity in Cross-Linked Liquid Crystalline Networks. *Adv. Mater.* **2017**, *29*, 1606509.
65. McBride, M. K.; Martinez, A. M.; Cox, L.; Alim, M.; Childress, K.; Beiswinger, M.; Podgorski, M.; Worrell, B. T.; Killgore, J.; Bowman, C. N. A readily programmable, fully reversible shape-switching material. *Sci. Adv.* **2018**, *4*, eaat4634.
66. Wang, Z. J.; He, Q. G.; Wang, Y.; Cai, S. Q. Programmable actuation of liquid crystal elastomers via ''living'' exchange reaction. *Soft Matter* **2019**, *15*, 2811-2816.

67. Jiang, Z.-C.; Xiao, Y.-Y.; Yin, L.; Han, L.; Zhao, Y. "Self-Lockable" Liquid Crystalline Diels–Alder Dynamic Network Actuators with Room Temperature Programmability and Solution Reprocessability. *Angew. Chem. Int. Ed.* **2020**, *59,* 4925-4931.
68. Valenzuela, C.; Chen, Y. H.; Wang, L.; Feng, W. Functional Liquid Crystal Elastomers Based on Dynamic Covalent Chemistry. *Chem. Eur. J.* **2022**, *28,* e202201957.
69. Kupfer, J.; Finkelmann, H. Nematic liquid single crystal elastomers. *Macromol. Rapid Commun.* **1991**, *12,* 717-726.
70. Wang, Y. C.; Huang, X. Z.; Zhang, J. Q.; Bi, M.; Zhang, J. D.; Niu, H. Y.; Li, C. S.; Yu, H. F.; Wang, B. S.; Jiang, H. R. Two-step crosslinked liquid-crystalline elastomer with reversible two-way shape memory characteristics. *Mol. Cryst. Liq. Cryst.* **2017**, *650,* 13-22.
71. Liu, Y. J.; Du, H. Y.; Liu, L. W.; Leng, J. S. Shape memory polymers and their composites in aerospace applications: a review. *Smart. Mater. Struct.* **2014**, *23,* 023001.
72. Yu, L.; Shahsavan, H.; Rivers, G.; Zhang, C.; Si, P. X.; Zhao, B. X. Programmable 3D Shape Changes in Liquid Crystal Polymer Networks of Uniaxial Orientation. *Adv. Funct. Mater.* **2018**, *28,* 1802809.
73. Barnes, M.; Verduzco, R. Direct shape programming of liquid crystal elastomers. *Soft Matter* **2019**, *15,* 870-879.
74. Lee, J.; Guo, Y. H.; Choi, Y.-J.; Jung, S.; Seol, D.; Choi, S.; Kim, J.-H.; Kim, Y.; Jeong, K.-U.; Ahn, S.-K. Mechanically programmed 2D and 3D liquid crystal elastomers at macro- and microscale via two-step photocrosslinking. *Soft Matter* **2020**, *16,* 2695-2705.
Wang, X. X.; Zhao, N.; Qin, B.; Xu, J. J.; Yang, W. L.; Li, C. S.; Sun, L. G.; Zhang, J. Q. Ultrasonics Sonochemistry Assisted Preparation of Polysiloxane Main-Chain Liquid-Crystalline Elastomers. *Macromol. Chem. Phys.* **2020**, *221,* 2000071.